Geomechanics and Engineering, *Vol. 16, No. 6 (2018) 569-575*
DOI: https://doi.org/10.12989/gae.2018.16.6.569

3D stability of shallow cavity roof with arbitrary profile under influence of pore water pressure

W.J. Luo[1] and X.L. Yang[*2]

[1]*School of Civil Engineering and Architecture, East China Jiaotong University, Nanchang, 330013, China*
[2]*School of Civil Engineering, Central South University, Changsha, 410075, China*

(Received April 22, 2018, Revised October 2, 2018, Accepted October 11, 2018)

Abstract. The stability of shallow cavities with an arbitrary profile is a difficult issue in geotechnical engineering. This paper investigates this problem on the basis of the upper bound theorem of limit analysis and the Hoek-Brown failure criterion. The influence of pore pressure is taken into consideration by regarding it as an external force acting on rock skeleton. An objective function is constructed by equating the internal energy dissipation to the external force work. Then the Lagrange variation approach is used to solve this function. The validity of the proposed method is demonstrated by comparing the analytical solutions with the published research. The relations between shallow and deep cavity are revealed as well. The detaching curve of cavity roof with elliptical profile is obtained. In order to facilitate the application of engineering practice, the numerical results are tabulated, which play an important role in tunnel design and stability analysis of roof. The influential factors on potential collapse are taken into consideration. From the results, the impact of various factors on the extent of detaching is seen intuitively.

Keywords: three-dimensional; shallow cavity; arbitrary profile; pore water pressure

1. Introduction

In order to alleviate the overcrowding of the urban space, underground space has been gradually utilized in recent decades. On one hand, as a result of good thermal insulation and groundwater retention, it enjoyed a rapid development. Underground structures, such as subways, underground squares and underground streets, are playing an increasingly important role in modern life (Yang and Wang 2018). On the other hand, along with the increase of underground structures, tremendous attention has been paid to the security and stability of them (Mollon and Dias 2009). Especially in urban centers where high-rise buildings grouped, the surface subsidence should be confined in a safety range to avoid significant casualties and economic losses. One of the most common forms of failures is the roof collapse of the underground structures. Compared to deep cavities, owing to the thinner overburden of shallow strata, the roof of shallow cavity is highly vulnerable to dynamic changes in boundary conditions and redistribution of stress near the cavity induced by excavation-related disturbances.

Large amounts of data from experiments have shown that the strength envelops of almost all geomaterials are nonlinear in the normal and shear stress space. A classical failure criterion representing this nonlinear feature is the Hoek-Brown failure criterion, which was proposed by Hoek and Brown (1980) and is a widely applied in geotechnical engineering (Yang *et al.* 2018). On the other hand, the upper bound theorem is a useful tool to solve the stability problems of geotechnical structures since it was introduced by Chen (1975). Based on the Hoek-Brown failure criterion and the limit analysis theory, Fraldi and Guarracino (2009) developed a curved failure mechanism. The analytical solution for the shape of the collapse region is derived by the calculus of variation. Subsequently, the equation of detaching curve with respect to tunnels with arbitrary excavation profiles is obtained by Fraldi and Guarracino (2010) in the same way. On the basis of previous works, the impending collapse was evaluated in circular tunnels by analytical and numerical approaches and progressive tunnel failure of tunnels. For the sake of further research and approaching the actual situation better, Huang (2012) developed three-dimensional failure mechanisms of deep rectangular and spherical cavity.

As mentioned above, the shallow cavity roof is more vulnerable than the deep. However, there are relatively few researches in this field (Jin and Gong 2017, Carranza-Torres and Reich 2017). Especially, when it comes to the three-dimensional shallow cavity, by now, it is still one of the most difficult tasks to provide reliable prediction of impending roof collapse. With the advance of the computer technology, the finite element method and other numerical calculation software have been widely used in this field. However, the construction of computational model and the selection of calculation parameters are still difficult problems, which can lead to irrational results. To enlarge the application scope of the study, the influence of pore water pressure is taken into consideration. Using variations principle, the analytical solution of detaching curve in shallow 3D-cavity with arbitrary profile subjected to pore water pressure is obtained. Through the comparison of analytic expressions, the validation of method proposed in

*Corresponding author, Professor
E-mail: csuyang@aliyun.com

ISSN: 2005-307X (Print), 2092-6219 (Online)

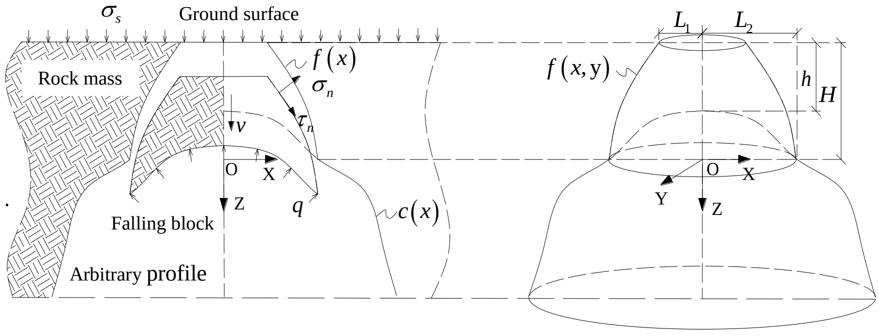

Fig. 1 3D rotational collapsing block above roof of shallow cavity with arbitrary profile

this paper is fully confirmed. In addition, the numerical results are tabulated in this literature for better application of engineering practice.

2. Theoretical background

2.1 Upper bound theorem of limit analysis

As introduced by Chen (1975), the upper bound theorem can be described as follows. The admissible actual load should not exceed the load derived by equating the external rate of work to the rate of energy dissipation in any kinematically admissible velocity field, which satisfy the velocity boundary condition. The specific formula can be written as

$$\int_v \sigma_{ij}^* \varepsilon_{ij}^* dv \geq \int_s T_i V_i ds + \int_v X_i V_i dv \tag{1}$$

where $\sigma_{ij}{}^*$ and $\varepsilon_{ij}{}^*$ are the stress tensor and strain rate in the kinematically admissible velocity field, respectively, v corresponds to the volume of the falling blocks, T_i is the surcharge load on the boundary s, X_i indicates the body force, and V_i is the velocity along the failure surface.

2.2 Hoek-Brown failure criterion

It is proved by plenty of experiments that the constitutive relationship of soil is nonlinear. The Hoek-Brown Failure Criterion was put forward (Hoek and Brown 1980) to represent this nonlinear feature. Compared to Mohr-Coulomb criterion, Hoek-Brown is more suitable for rock mass. Therefore, it is widely used in tunnels and slopes (Fahimifar *et al.* 2015, Lee 2016, Senent and Mollon 2013, Li and Yang 2018a, b, Yang and Liu 2018). In the majority of cases, the Criterion is generally written in form of maximum and minimum effective principle stresses. In this article, however, it is represented by normal and shear stresses, for the simple reason that the energy dissipation on the velocity discontinuity surface consists of two components induced by normal stress and shear stress separately. That is (Hoek and Brown 1997)

$$\tau = A\sigma_{ci}\left(\frac{\sigma_n - \sigma_{tm}}{\sigma_{ci}}\right)^B \tag{2}$$

where τ is the shear stress along the failure surface, A and B are dimensionless material constants, σ_{ci} represents the uniaxial compressive strength, σ_n is the normal stress of failure surface, and σ_{tm} is the tensile strength of the rock mass. It should be point out that Hoek-Brown failure criterion can be simplified exactly down to Mohr-Coulomb failure criterion when the condition that $\{B = 1, A = \tan\phi, \sigma_{tm} = c/\tan\phi\}$ is met. The nonlinear failure criterion is widely used in engineering (Agar *et al.* 1985, Anyaegbunam 2015, Serrano anlalla 1999, Sofianos and Halakatevakis 2002, Xu *et al.* 2018, Yang and Li 2018b).

3. Failure mechanism of shallow cavity with arbitrary shape

The analytical solutions of failure mechanism to estimate the collapsing block range over the deep 2D tunnel was proposed by Fraldi and Guarracino (2009, 2010). However, as a matter of fact, the stress state of almost all underground structures is three-dimensional, and corresponding simplification to a plain-strain condition will lead to an inappropriate result. For this reason, three-dimensional failure mechanisms of deep spherical cavity were developed by Huang (2012). Due to the thinner overburden soil layer, the stability of shallow buried is largely smaller than that of deep buried, What's more, little research has been done for this field. In this paper, the roof stability of shallow cavity with arbitrary profile $c(x)$ is considered. Considering the symmetry, the practical failure characteristics of theses shallow cavity roofs is regarded as a 3D rotation. Similar to the case in 2D, the velocity discontinuity line is described as an unknown $f(x)$ indicating failure curve in the XOZ coordinate.

As shown in Fig. 1, by rotating $f(x)$ and $c(x)$ around the Z axis for 360 degrees, the 3D failure mode including a collapsing block and a roof detaching surface is formed. L_1 and L_2 correspond half width of the top and bottom of failure block respectively. h indicates the thickness of overburden soil layer, σ_s is surface load and q is the supporting pressure of the lining. To facilitate the application of engineering practice, the example of cavity with elliptical profile is calculated. For its flexibility, when the minor axis of an ellipse approaches to zero, it represents a rectangular cavity. When the long axis equals minor axis of an ellipse, it turns into a circle, which was introduced by Huang (2012).

4. Upper bound analysis of shallow cavity roof

According to theory of limit analysis, the calculation of external work and internal energy dissipation is employed (Aminpour *et al.* 2018, Li and Yang 2018c, Xu and Yang 2018, Yang and Li 2018a, c, Yang and Zhang 2018). With the combination of Hoek-Brown criterion and flow rules, the energy dissipation per unit area on the detaching surface caused by normal stress-strain and shear stress-strain can be written as

$$D=\sigma_n\dot{\varepsilon}_n+\tau_n\dot{\gamma}_n=\left\{\sigma_{tm}-\sigma_{ci}\left[ABf'(x)\right]^{\frac{1}{1-B}}\left(1-B^{-1}\right)\right\}\frac{1}{\sqrt{1+f'(x)^2}}v \quad (3)$$

where $\dot{\varepsilon}_n$ and $\dot{\gamma}_n$ are the normal and shear plastic strain rate, respectively, $f(x)$ is the analytical formula of failure curve, $f'(x)$ is the first derivative of $f(x)$. v represents the velocity of the Collapse block. Applying the formula for the area of a rotating body, the lateral area of the rotational solid S can be derived as follows

$$S=2\pi\int_{L_1}^{L_2}x\sqrt{1+f'(x)^2}dx \quad (4)$$

where L_1 and L_2 are the upper and lower half width of the detaching curve. Through integral, the total energy dissipation along the detaching surface is

$$P_D=2\pi\int_{L_1}^{L_2}\left\{\sigma_{tm}-\sigma_{ci}\left[ABf'(x)\right]^{\frac{1}{1-B}}\left(1-B^{-1}\right)\right\}xvdx \quad (5)$$

To obtain the power of weight for the detaching volume, the volume is calculated through integral first and then it is multiplied by the bulk density and the velocity of the impending block, that is

$$P_\gamma=\gamma\int_{L_1}^{L_2}\pi x^2 f'(x)vdx-\gamma\int_0^{L_2}\pi x^2 c'(x)vdx \quad (6)$$

where γ is bulk density of rocks, $c(x)$ denotes the arbitrary cavity roof profile.

The work rate of cavity roof, as shown in Fig. 1, produced by supporting pressure over the velocity field can be expressed as follows

$$P_q=-q\int_0^{L_2}2\pi xv\sqrt{1+c'^2(x)}\Big/\sqrt{1+c'^2(x)}dx=-\pi L_2^{\,2}qv \quad (7)$$

in which q corresponds to the supporting pressure of the shallow cavity roof. Different from the deep buried cavity, when the failure surface extends to the surface (Augarde and Lyamin 2003), the surface load should be taken into consideration. The power of surface load is given as

$$P_{\sigma_s}=\pi L_1^{\,2}\sigma_s v \quad (8)$$

where σ_s is the pressure of surface.

In order to estimate effect of pore water pressure in the framework of the upper bound theorem of limit analysis for slope stability, the formula calculating the work rate of the collapse block pore water pressure was introduced by Viratjandr and Michalowski (2006), which can be written as follows

$$P_u=-\int_s un_iv_ids=-2\pi\int_{L_1}^{L_2}r_u\gamma f(x)xvdx \quad (9)$$

where r_u is the pore water pressure coefficient.

For the purpose of obtaining the upper bound solution of shallow cavity roof with arbitrary profile under the influence of pore water pressure, limit equilibrium is established by equating the rate of energy dissipation to the external rate of work. In order to find the analytical expression of unknown function $f(x)$, an objective function ξ should be written in the functional form of $f(x)$

$$\xi\left[f(x),f'(x),x\right]=P_D-P_\gamma-P_q-P_{\sigma_s}-P_u \quad (10)$$

Substituting the Eqs. (5)-(9) into Eq. (10), the expression of objective function is obtained

$$\begin{aligned}\xi&=2\pi\int_{L_1}^{L_2}\left\{\left\{\sigma_{tm}+r_u\gamma f(x)-\sigma_{ci}\left[ABf'(x)\right]^{\frac{1}{1-B}}\left(1-B^{-1}\right)\right\}x-\frac{\gamma}{2}x^2f'(x)\right\}vdx\\&\quad+\gamma\int_0^{L_2}\pi x^2c'(x)vdx+\pi L_2^{\,2}qv-\pi L_1^{\,2}\sigma_sv\\&=2\pi\int_{L_1}^{L_2}\psi\left[f(x),f'(x),x\right]vdx+\gamma\int_0^{L}\pi x^2c'(x)vdx+\pi L_2^{\,2}qv-\pi L_1^{\,2}\sigma_sv\end{aligned} \quad (11)$$

For simplifying the calculation procedure, $\psi\left[f(x),f'(x),x\right]$, part of ξ associated with $f(x)$, is extracted. That is

$$\psi\left[f(x),f'(x),x\right]=\left\{\sigma_{tm}+r_u\gamma f(x)-\sigma_{ci}\left[ABf'(x)\right]^{\frac{1}{1-B}}\left(1-B^{-1}\right)\right\}x-\frac{\gamma}{2}x^2f'(x) \quad (12)$$

On the basis of upper bound theorem of limit analysis, the optimum solution of $f(x)$ can be obtained when the function ξ approaches the extremum. According to Lagrange calculus of variations, the problem of solving the extreme value and the maximum of a function can be converted into solving the following differential equation

$$\frac{\partial\psi}{\partial f(x)}-\frac{d}{dx}\left[\frac{\partial\psi}{\partial f'(x)}\right]=0 \quad (13)$$

The first-order partial derivatives of the Eq. (12) can be written as follows

$$\frac{\partial\psi}{\partial f(x)}=r_u\gamma x \quad (14)$$

$$\frac{\partial\psi}{\partial f'(x)}=\sigma_{ci}(AB)^{\frac{1}{1-B}}B^{-1}\left[f'(x)\right]^{\frac{B}{1-B}}x-\frac{\gamma}{2}x^2 \quad (15)$$

Substituting Eqs. (14) and (15) into Eq. (13), and then integrating both sides of the equation, the first derivative of $f(x)$ is obtained as

$$f'(x)=A^{-\frac{1}{B}}B^{-1}\left[\frac{(1+r_u)\gamma}{2\sigma_{ci}}\right]^{\frac{1-B}{B}}x^{\frac{1-B}{B}} \quad (16)$$

By integrating Eq. (16), the explicit solution of the detaching curve above the cavity roof, $f(x)$, is derived as

$$f(x)=A^{-\frac{1}{B}}\left[\frac{(1+r_u)\gamma}{2\sigma_{ci}}\right]^{\frac{1-B}{B}}x^{\frac{1}{B}}-c_1 \tag{17}$$

According to the geometric boundary conditions of collapse curve, following boundary constraints should be satisfied

$$\begin{cases} f(x=L_1)=-H \\ f(x=L_2)=0 \end{cases} \tag{18}$$

Regarding the shallow cavity, we usually know h which represents the buried depth of the cavern. As is shown in the Fig. 1, H is thickness of detaching block

$$H=h-c(0) \tag{19}$$

Substituting Eq. (17) into Eq. (18), c_1 and L_1 can be represented by L_2

$$\begin{cases} c_1=\left[\frac{(1+r_u)\gamma}{2\sigma_{ci}}\right]^{\frac{1-B}{B}}A^{-\frac{1}{B}}L_2^{\frac{1}{B}} \\ L_1=\left\{L_2^{\frac{1}{B}}-H\left[\frac{(1+r_u)\gamma}{2\sigma_{ci}}\right]^{\frac{B-1}{B}}A^{\frac{1}{B}}\right\}^{B} \end{cases} \tag{20}$$

Plugging the expression of c_1 shown in Eq. (20) into the Eq. (17), the analytical formula of failure curve $f(x)$ can be obtained. By rotating the 2D detaching curve $f(x)$ around the Z-axis, the 3D failure surface is formed. The analytical formula of 3D velocity discontinuity surface can be written as follows

$$z=\left[\frac{(1+r_u)\gamma}{2\sigma_{ci}}\right]^{\frac{1-B}{B}}A^{-\frac{1}{B}}\left(x^2+y^2\right)^{\frac{1}{2B}}-\left[\frac{(1+r_u)\gamma}{2\sigma_{ci}}\right]^{\frac{1-B}{B}}A^{-\frac{1}{B}}L_2^{\frac{1}{B}} \tag{21}$$

As seen from the above expression, the lower half width of the detaching curve L_2 is still unknown. To solve L_2, one more equation should be introduced. According to the principle of virtual work, the total power which induced by plastic deformation and external force equals to zero in the admissible velocity filed. Commanding function ξ equal to zero, and then substituting Eq. (16) and Eq. (17) into Eq. (11), the equation, ξ=0, containing the only unknown geometric parameter L_2 is obtained.

$$\begin{aligned}\xi&=\pi\left(\sigma_{tm}-r_u\gamma c_1\right)\left(L_2^2-L_1^2\right)v+\pi L_2^2qv-\pi L_1^2\sigma_s v+\gamma\int_0^{L_2}\pi x^2c'(x)vdx\\&+\frac{2\pi B}{2B+1}\sigma_{ci}^{\frac{B-1}{B}}A^{-\frac{1}{B}}\left(\frac{\gamma}{2}\right)^{\frac{1}{B}}(1+r_u)^{\frac{1-B}{B}}\left[\frac{(B+1)r_u}{B}-1\right]\left(L_2^{\frac{2B+1}{B}}-L_1^{\frac{2B+1}{B}}\right)v\\&=0\end{aligned} \tag{22}$$

With the help of numerical analysis software, the geometric parameter L_2 can be derived by the transcendental equation above. Along with the substitution of L_2, the analytical solution of detaching curve in shallow 3D-cavity with arbitrary profile subjected to pore water pressure is solved completely.

5. Comparisons and numerical results

5.1 Comparisons

In this paper, detaching curve in shallow 3D-cavity with arbitrary profile subjected to pore water pressure is drawn. In order to validate the results of this paper, the solutions of Guan and Zhu (2017) will be used for comparison, in which deep 3D-cavity without pore water pressure and the pressure of surface is taken into consideration. For better contrast, the pore water pressure coefficient r_u and the upper half width of the detaching curve L_1 are supposed to zero. Plugging the expression r_u=0 and L_1=0 into Eq. (22), the result can be simplified as follows

$$\xi=\pi\sigma_{tm}L_2^2v+\pi L_2^2qv+\gamma\int_0^{L_2}\pi x^2c'(x)vdx-\frac{2\pi B}{2B+1}\sigma_{ci}^{\frac{B-1}{B}}A^{-\frac{1}{B}}\left(\frac{\gamma}{2}\right)^{\frac{1}{B}}L_2^{\frac{2B+1}{B}}v \tag{23}$$

From the expression above, it is same as solution of proposed by Guan and Zhu (2017). It is worth noting that, for shallow cavity, the L_1 decreases with the increase of the buried depth of the cavern when other parameters are fixed. L_1 approaches to 0, when h reaches cut-off point of deep cavities. At this moment, the deep 3D-cavity, to some extent, can be regarded as a special case of shallow cavity, in which r_u=0 and L_1=0.

Comparing with the previous solutions, the three-dimensional failure mechanism of a rectangular cavity was studied. On the basis of Eq. (23), rectangular cavity can be considered as $c(x)$=0. The following expression can be obtained

$$\xi=\pi\sigma_{tm}L_2^2v+\pi L_2^2qv-\frac{2\pi B}{2B+1}\sigma_{ci}^{\frac{B-1}{B}}A^{-\frac{1}{B}}\left(\frac{\gamma}{2}\right)^{\frac{1}{B}}L_2^{\frac{2B+1}{B}}v \tag{24}$$

The expression of shallow 3D-cavity convert into the expression of three-dimensional failure mechanism of a rectangular cavity.

From the comparisons, not only the validity of the failure mechanism of shallow 3D-cavity presented in this paper is evaluated, but the wide range of methods used in this paper is fully illustrated as well.

5.2 Numerical results of elliptic rotating surface

The detaching block over the shallow cavity roof with arbitrary profile under the influence of pore water pressure can be evaluated in the method mentioned above. In actual engineering, the majority of underground cavity roofs are planar and dome shaped. To enlarge the applying scope in practical engineering, shallow cavity with elliptical profile is calculated.

As shown in Fig. 2, a represents one of semi-axis which rotating around the Z, and another semi-axis b indicates dome height. In this way, the analytical expression of an ellipse $c(x)$ can be expressed by a and b. The first derivative of $c(x)$ can be written as follows

$$c'(x)=\frac{b}{a}\frac{x}{\sqrt{a^2-x^2}} \tag{25}$$

To solve the equation ξ=0, the unknown integral part

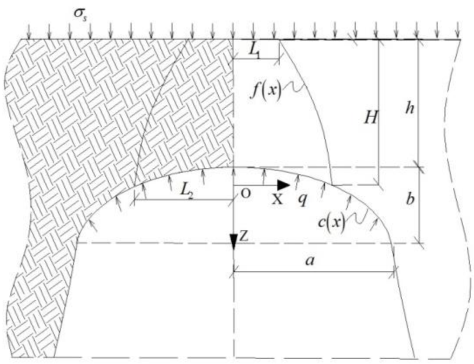

Fig. 2 The sectional drawing of shallow cavity with elliptical profile

Table 1 The collapsing range with regard to different parameters

$a(m)$	$b(m)$	γ_u	$L_1(m)$	$L_2(m)$	$P(10^3\,\mathrm{kN})$
10	5.0	0.1	0.811	4.377	2.465
15	5.0	0.1	0.637	4.099	2.152
20	5.0	0.1	0.588	4.020	2.069
25	5.0	0.1	0.567	3.987	2.033
30	5.0	0.1	0.556	3.969	2.015
15	0.0	0.1	0.531	3.930	1.974
15	2.5	0.1	0.582	4.011	2.059
15	5.0	0.1	0.637	4.099	2.152
15	7.5	0.10	0.696	4.195	2.258
15	10.0	0.10	0.760	4.300	2.377
15	5.0	0.00	0.969	4.389	2.824
15	5.0	0.05	0.809	4.242	2.466
15	5.0	0.10	0.637	4.099	2.152
15	5.0	0.15	0.433	3.958	1.827
15	5.0	0.20	0.192	3.817	1.627

M in Eq. (22), can be expressed in the following form

$$M=\gamma\int_0^{L_2}\pi x^2 c'(x)dx=\frac{\pi\gamma}{3a}\left[2a^3b-b\left(2a^2+L_2{}^2\right)\sqrt{a^2-L_2{}^2}\right] \quad (26)$$

By substituting Eq. (26) into Eq. (22), L_2 can be solved. So combining Eq. (20) makes it possible to calculate L_1. Collapsing weight P can be known from the Eq. (6), which can be expressed as follows

$$P=\gamma\int_{L_1}^{L_2}\pi x^2 f'(x)dx-\gamma\int_0^{L_2}\pi x^2 c'(x)dx \quad (27)$$

As the geometric determinant variables for the collapse of falling block, L_1 and L_2 are taken into consideration. Similarly, as an intuitive response to mechanics, collapsing weight P should also be the focus of the study. Because of the multitudinous influencing factors for the failure, a few more representative are chosen to carry on the analysis.

To facilitate the reference to practical engineering, the numerical results are tabulated in Table 1 As shown in Table 1, it is obvious that with the increase of b, the results of L, h and P under investigation increase too. Inversely, these

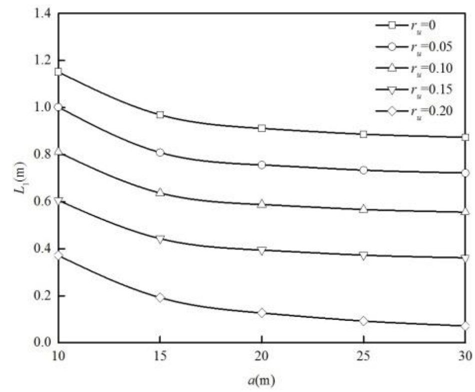

(a) Upper collapsing width with different half ceiling span a

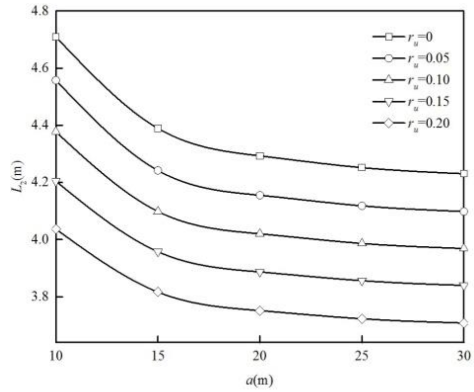

(b) Lower collapsing width with different half ceiling span a

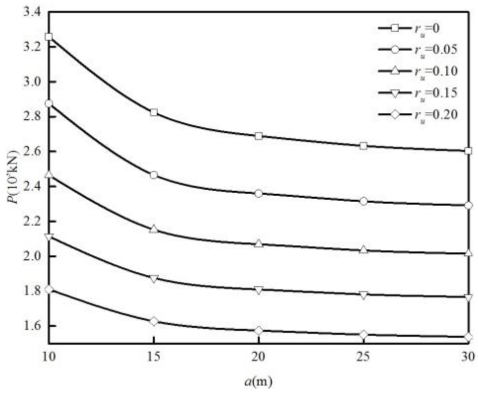

(c) Collapsing weight with different half ceiling span a

Fig. 3 The collapsing range for different half ceiling span a

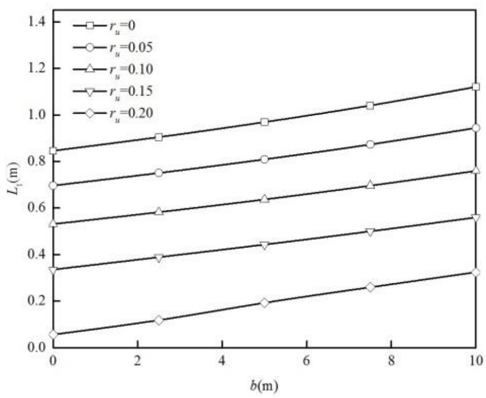

(a) The upper collapsing width with different ceiling height b

Fig. 4 The collapsing range for different ceiling height b

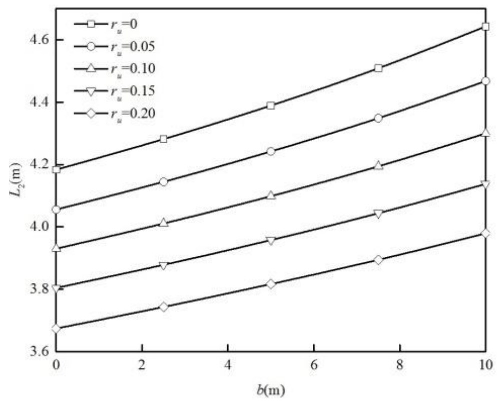

(b) The lower collapsing width with different ceiling height b

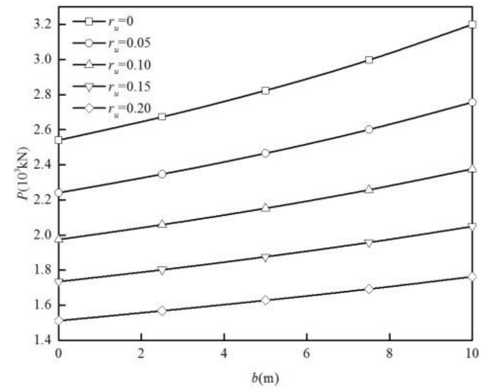

(c) The collapsing weight with different ceiling height b

Fig. 4 Continued

results of them decease with the larger magnitude of a and r_u. When the other parameters are fixed on A=0.3, B=0.7, γ=25 kN/m^3, σ_{ci}=0.5 MPa, σ_{tm}=σ_{ci}/100, σ_s=40 kPa, q=10 kPa and h=4 m.

For the purpose of facilitating the observation of changes between variables studied, these figures are drawn. Fig. 3 illustrates the effects of the half ceiling span a and the pore water pressure coefficient r_u on upper and lower half width of the detaching curve L_1, L_2 and collapsing weight P, corresponding to the ceiling height b= 5m. It is found that when the half ceiling span a is small, the dependent variables L_1, L_2 and P change obviously. They decrease with increasing ceiling span a. When the half ceiling span a is greater than 50m, there are almost no change in L_1, L_2 and P. According to the results, it can be seen the greater the magnitudes of r_u and a are, the smaller the collapsing range.

Employing similar approach, the Fig. 4 shows changes in L_1, $L_2$and P corresponding to half ceiling span a=15 m, ceiling height b varying from 0 to 10m and pore water pressure coefficient r_u from 0 to 0.2. It is found that collapsing range tends to increase with the increase of ceiling height b, however, the collapsing range decrease as the pore water pressure coefficient r_u increases. From an engineering standpoint, it is worth mentioning that different from deep underground space, owing to the thinner overburden of shallow strata which cannot form a complete arch, the shallow cavity roof is highly vulnerable to dynamic changes in boundary conditions and redistribution of stress near the cavity induced by excavation-related disturbances. Moreover, at the condition that other factors are fixed, the higher ceiling height b means the greater quantity of rock and soil mass over the shallow cavity roof. A part of the excess is counted as the falling block as well. That is the reason why the collapsing range tends to increase with the increase of ceiling height b.

In combination with Figs. 3 and 4, the relationship between them can be easily found. It can be found from Figs. 3 and 4 that when the pore water pressure coefficient is uniform, the collapsing range represented by L_1, L_2 and P decreases as ceiling span increases and tends to stationary value. From the perspective of geometry, when the ceiling span reaches infinity, the roof becomes a plane. As mentioned earlier, similarly, when b=0, this is also the case in Figs. 3 and 4. So the final stationary value shown in Fig. 3 can be expressed as the corresponding initial values of Fig. 4. These also show that the present results are effective.

5. Conclusions

Based on the Hoek–Brown failure criterion and the upper bound theorem, the analytical solution of detaching curve in shallow 3D-cavitywith arbitrary profile subjected to pore water pressure is studied. The analytical solution of detaching curve subjected to pore water pressure can be regarded that the bulk density of rocks γ is replaced by $(1+r_u)\gamma$ compared with the case without pore water pressure. When the pore water pressure coefficient is uniform, the collapsing range represented by L_1, L_2 and P decreases as ceiling span increases and tends to stationary value. When the pore water pressure increases, both the height and the width of collapsing block decrease while the shape of collapsing block remains unchanged.

From the comparison between the deep and shallow cavity, the deep 3D-cavity, to some extent, can be regarded as a special case of shallow cavity, in which L_1=0. Through the simplification of the equation, the formula deduced from the previous research has been obtained. Therefore, the formula for shallow cavity has a wider scope of application than that of deep cavity.

Acknowledgements

Financial support received from the National Natural Science Foundation (51768022) and project (20181BCB24011) for the preparation of this manuscript is greatly appreciated.

References

Agar, J.G., Morgenstern, N.R. and Scott, J. (1985), "Shear strength and stress-strain behavior of Athabasca oil sand at elevated temperatures and pressure", *Can. Geotech. J.*, **24**(1), 1-10.

Aminpour, M.M., Maleki, M. and Ghanbari, A. (2017), "Investigation of the effect of surcharge on behavior of soil slopes", *Geomech. Eng.*, **13**(4), 653-669.

Anyaegbunam, A.J. (2015), "Nonlinear power-type failure laws for geomaterials: Synthesis from triaxial data, properties, and applications", *Int. J. Geomech.*, **15**(1), 04014036.

Augarde, C.E., Lyamin, A.V. and Sloan, S.W. (2003), "Prediction of undrained sinkhole collapse", *J. Geotech. Geoenviron. Eng.*, **129**(3), 197-205.

Carranza-Torres, C. and Reich, T. (2017), "Analytical and numerical study of the stability of shallow underground circular openings in cohesive ground", *Eng. Geol.*, **226**, 70-92.

Chen, W.F. (1975), *Limit Analysis and Soil Plasticity*, Elsevier.

Fahimifar, A., Ghadami, H. and Ahmadvand, M. (2015), "The ground response curve of underwater tunnels, excavated in a strain-softening rock mass", *Geomech. Eng.*, **8**(3), 323-359.

Fraldi, M. and Guarracino, F. (2009), "Limit analysis of collapse mechanisms in cavities and tunnels according to the Hoek-Brown failure criterion", *Int. J. Rock Mech. Min. Sci.*, **46**(4), 665-673.

Fraldi, M. and Guarracino, F. (2010), "Analytical solutions for collapse mechanisms in tunnels with arbitrary cross sections", *Int. J. Solid. Struct.*, **47**(2), 216-223.

Guan, K., Zhu, W.C., Niu, L.L. and Wang, Q.Y. (2017), "Three-dimensional upper bound limit analysis of supported cavity roof with arbitrary profile in Hoek-Brown rock mass", *Tunn. Undergr. Sp. Technol.*, **69**, 147-154.

Hoek, E. and Brown, E.T. (1980), "Empirical strength criterion for rock masses", *J. Geotech. Eng. Div.*, **106**(9), 1013-1035.

Hoek, E. and Brown, E.T. (1997), "Practical estimates of rock mass strength", *Int. J. Rock Mech. Min. Sci.*, **34**(8), 1165-1186.

Huang, F. (2012), "Upper bound analysis of collapsing mechanism of surrounding rock and rockbolt supporting structures for tunnels", Ph.D. Thesis, Central South University, Changsha, China.

Jin, S., Jin, J. and Gong, Y. (2017), "Natural ventilation of urban shallowly-buried road tunnels with roof openings", *Tunn. Undergr. Sp. Technol.*, **63**, 217-227.

Lee, Y.J. (2016), "Determination of tunnel support pressure under the pile tip using upper and lower bounds with a superimposed approach", *Geomech. Eng.*, **11**(4), 587-605.

Li, Y.X. and Yang, X.L. (2018a), "Three-dimensional seismic displacement analysis of rock slopes based on Hoek-Brown failure criterion", *KSCE J. Civ. Eng.*, **22**(11), 4334-4344.

Li, Z.W. and Yang, X.L. (2018b), "Stability of 3D slope under steady unsaturated flow condition", *Eng. Geol.*, **242**, 150-159.

Li, Z.W. and Yang, X.L. (2018c), "Active earth pressure for soils with tension cracks under steady unsaturated flow conditions", *Can. Geotech. J.*, **55**(12), 1850-1859.

Mollon, G. and Dias, D. (2009), "Probabilistic analysis of circular tunnels in homogeneous soil using response surface methodology", *J. Geotech. Geoenviron. Eng.*, **135**(9), 1314-1325.

Senent, S., Mollon, G. and Jimenez, R. (2013), "Tunnel face stability in heavily fractured rock masses that follow the Hoek-Brown failure criterion", *Int. J. Rock Mech. Min. Sci.*, **60**(2), 440-451.

Serrano, A. and Olalla, C. (1999), "Tensile resistance of rock anchors", *Int. J. Rock Mech. Min. Sci.*, **36**(4), 449-474.

Sofianos, A.I. and Halakatevakis, N. (2002), "Equivalent tunnelling Mohr-Coulomb strength parameters from given Hoek-Brown ones", *Int. J. Rock Mech. Min. Sci.*, **39**(1), 131-137.

Viratjandr, C. and Michalowski, R.L. (2006), "Limit analysis of submerged slopes subjected to water drawdown", *Can. Geotech. J.*, **43**(8), 802-814.

Xu, J.S. and Yang, X.L. (2018), "Three-dimensional stability analysis of slope in unsaturated soils considering strength nonlinearity under water drawdown", *Eng. Geol.*, **237**, 102-115.

Xu, J.S., Li, Y.X. and Yang, X.L. (2018), "Seismic and static 3D stability of two-stage slope considering joined influences of nonlinearity and dilatancy", *KSCE J. Civ. Eng.*, **22**(10), 3827-3836.

Yang, X.L. and Li, Z.W. (2018c), "Upper bound analysis of 3D static and seismic active earth pressure", *Soil Dyn. Earthq. Eng.*, **108**, 18-28.

Yang, X.L. and Liu, Z.A. (2018), "Reliability analysis of three-dimensional rock slope", *Geomech. Eng.*, **15**(6), 1183-1191.

Yang, X.L. and Zhang, S. (2018), "Risk assessment model of tunnel water inrush based on improved attribute mathematical theory", *J. Central South Univ.*, **25**(2), 379-391.

Yang, X.L. and Li, Z.W. (2018a), "Factor of safety of three-dimensional stepped slopes", *Int. J. Geomech.*, **18**(6), 04018036.

Yang, X.L. and Li, Z.W. (2018b), "Kinematical analysis of 3D passive earth pressure with nonlinear yield criterion", *Int. J. Numer. Anal. Meth. Geomech.*, **42**(7), 916-930.

Yang, X.L. and Wang, H.Y. (2018), "Catastrophe analysis of active-passive mechanisms for shallow tunnels with settlement", *Geomech. Eng.*, **15**(1), 621-630.

Yang, X.L., Zhou, T. and Li, W.T. (2018), "Reliability analysis of tunnel roof in layered Hoek-Brown rock masses", *Comput. Geotech.*, **104**, 302-309.

CC